Emerin induces nuclear breakage in *Xenopus* extract and early embryos

Matthew R. Dilsaver[a], Pan Chen[a], Trey A. Thompson[a], Traci Reusser[b], Richik N. Mukherjee[a], John Oakey[b], and Daniel L. Levy[a],*
[a]Department of Molecular Biology and [b]Department of Chemical Engineering, University of Wyoming, Laramie, WY 82071

ABSTRACT Emerin is an inner nuclear membrane protein often mutated in Emery–Dreifuss muscular dystrophy. Because emerin has diverse roles in nuclear mechanics, cytoskeletal organization, and gene expression, it has been difficult to elucidate its contribution to nuclear structure and disease pathology. In this study, we investigated emerin's impact on nuclei assembled in *Xenopus laevis* egg extract, a simplified biochemical system that lacks potentially confounding cellular factors and activities. Notably, these extracts are transcriptionally inert and lack endogenous emerin and filamentous actin. Strikingly, emerin caused rupture of egg extract nuclei, dependent on the application of shear force. In egg extract, emerin localized to nonnuclear cytoplasmic membranes, and nuclear rupture was rescued by targeting emerin to the nucleus, disrupting its membrane association, or assembling nuclei with lamin A. Furthermore, emerin induced breakage of nuclei in early-stage *X. laevis* embryo extracts, and embryos microinjected with emerin were inviable, with ruptured nuclei. We propose that cytoplasmic membrane localization of emerin leads to rupture of nuclei that are more sensitive to mechanical perturbation, findings that may be relevant to early development and certain laminopathies.

INTRODUCTION

Mutations in proteins of the nuclear envelope (NE) are increasingly being implicated in a host of diseases, generally termed nuclear envelopathies or laminopathies (Prokocimer *et al.*, 2009; Worman *et al.*, 2010; Burke and Stewart, 2014; Davidson and Lammerding, 2014; Janin *et al.*, 2017). Emerin (gene symbol *EMD*) is an important member of this group, as its mutation accounts for ~60% of cases of Emery–Dreifuss muscular dystrophy (EDMD) (Bione *et al.*, 1994; Helbling-Leclerc *et al.*, 2002; Koch and Holaska, 2014; Janin *et al.*, 2017). Emerin is an integral membrane protein found at the inner nuclear membrane where it binds directly to A- and B-type nuclear lamins (Gruenbaum *et al.*, 2005; Barton *et al.*, 2015). Emerin belongs

to the LEM domain (Lap2, emerin, Man1 domain) protein family, whose members share a common sequence motif that mediates indirect interactions with chromatin, and emerin interacts with other LEM domain proteins as well as with itself (Haraguchi *et al.*, 2001; Lee *et al.*, 2001; Segura-Totten *et al.*, 2002; Shimi *et al.*, 2004; Bengtsson and Wilson, 2006; Holaska and Wilson, 2007; Wilson and Foisner, 2010; Berk *et al.*, 2013, 2014). While emerin and the nuclear lamina are implicated in many functions, ranging from chromatin organization and transcription regulation to nuclear mechanics and signaling, important questions remain about how emerin controls nuclear structure and how emerin mutations give rise to disease phenotypes.

Emerin plays diverse roles in nuclear structure, actin dynamics, mechanosensation, and gene expression. Emerin knockdown in cardiomyocytes decreased nuclear invaginations and increased nuclear size (Shimojima *et al.*, 2017). In mouse embryonic fibroblasts, emerin deletion resulted in abnormal nuclear shape (Lammerding *et al.*, 2005), and altered actin dynamics caused by deletion or mutation of lamin A could be rescued by ectopic emerin expression (Ho *et al.*, 2013). Further evidence for emerin's impact on the actin cytoskeleton came from in vitro studies showing that emerin can increase actin polymerization, potentially impacting the dynamics of the intranuclear actin network (Holaska *et al.*, 2004). Emerin also functions

in actin-mediated nuclear positioning and cell migration (Chang *et al.*, 2013). At the inner nuclear membrane, emerin interacts with SUN domain proteins, components of the LINC (linkers of the nucleoskeleton to the cytoskeleton) complexes that transduce mechanical signals across the NE (Razafsky and Hodzic, 2009; Haque *et al.*, 2010; Tapley and Starr, 2013; Zuela and Gruenbaum, 2016). Consistent with emerin functioning in mechanosensation, emerin-deficient mouse embryonic fibroblasts showed reduced expression of mechanosensitive genes under mechanical strain, ultimately resulting in apoptosis (Lammerding *et al.*, 2005). In addition, nuclei lacking emerin exhibited altered NE elasticity and mechanical response to applied force, which might explain the increased fragility of EDMD nuclei (Rowat *et al.*, 2006; Guilluy *et al.*, 2014). Emerin also plays important roles in regulating gene expression and chromatin organization (Haraguchi *et al.*, 2004; Holaska *et al.*, 2006; Markiewicz *et al.*, 2006; Demmerle *et al.*, 2012; Le *et al.*, 2016; Willer and Carroll, 2017).

Here we investigate emerin's impact on nuclear structure, using *Xenopus laevis* egg extract, a simplified system with many advantages. First, *Xenopus* eggs and early embryos do not express emerin (Gareiss *et al.*, 2005), allowing us to test the effect of ectopic emerin addition. Second, it is simple to manipulate *Xenopus* egg extract biochemically; for instance, a recombinant protein of interest, such as emerin, can be added directly. Third, extracts are composed of stockpiled egg proteins and membrane that support de novo nuclear assembly upon addition of demembranated *Xenopus* sperm chromatin, and these nuclei can be subjected to typical studies of nuclear structure and function (Chen and Levy, 2018). Fourth, these extracts lack filamentous actin and are transcriptionally inert, eliminating potentially confounding effects of emerin on actin dynamics and transcription, respectively. Furthermore, complementary in vivo studies using *Xenopus* embryos are possible. While *Xenopus* egg extracts have been used to investigate the mitotic phosphorylation of emerin (Hirano *et al.*, 2005) and the localization of emerin's LEM domain (Dreger *et al.*, 2002), in this study we investigate the impact of full-length emerin on both in vitro assembled nuclei and embryonic nuclei.

RESULTS
Emerin induces breakage of nuclei assembled in *Xenopus* egg extract
Emerin protein expression is not detectable in *X. laevis* until stage 43, when swimming tadpoles have already developed (Gareiss *et al.*, 2005). As *Xenopus* eggs and early embryos do not contain endogenous emerin protein, something we confirmed by Western blot (Supplemental Figure S1A), we first asked how ectopic addition of emerin to *Xenopus* egg extract would influence nuclear structure and morphology. To our surprise, addition of recombinant emerin to nuclei assembled in *Xenopus* egg extract resulted in apparent nuclear rupture. Control nuclei treated with the dialysis buffer used in the final step of emerin purification exhibited Hoechst-stained DNA encased in a spherical or ellipsoid nucleus, as expected. When nuclei were treated with emerin, the DNA was converted into elongated strings and/or puncta that spread across the entire field of view (Figure 1, A and B). As a control, we heat-treated emerin at two different temperatures. Emerin inactivated at 100°C for 5 min was no longer capable of inducing the stringy DNA phenotype, while 60°C-treated emerin was still active in our assay, suggesting some level of heat resistance (Supplemental Figure S1B). We also tested a range of emerin concentrations and incubation times, observing nuclear rupture with 0.6–5 nM emerin and as little as 15 min of incubation (Supplemental Figure S1, C and D).

While the stringy/punctate DNA phenotype was striking, we also noted some apparently intact nuclei after emerin treatment. To quantify this observation, we incubated in vitro–assembled nuclei with the import substrate GST-GFP-NLS prior to emerin addition. We then counted the number of intact nuclei that still retained intranuclear GFP-NLS signal. On the basis of experiments with eight different egg extracts, we observed that more than 50% of emerin-treated nuclei were disrupted (Figure 1C) and only 18% of nuclei lost GFP-NLS signal upon treatment with heat-inactivated emerin (unpublished data). To further confirm nuclear breakage, we showed that nuclei and DNA in emerin-treated samples accumulated GFP-cGAS (Supplemental Figure S1E), a cytoplasmic DNA binding protein that is excluded from intact nuclei (Raab *et al.*, 2016). Furthermore, stringy DNA from ruptured nuclei showed little to no staining for membrane (Figure 2A), nucleoporins (Supplemental Figure S2, A and B), or Man1 (Supplemental Figure S2C), reflecting complete dissolution of the NE. Man1 is a LEM domain protein that is present in *X. laevis* eggs and early embryos (Reil and Dabauvalle, 2013). Man1 staining was unaffected in intact emerin-treated nuclei (Supplemental Figure S2C), suggesting that excess emerin is not negatively influencing the localization of other LEM domain proteins.

Our data suggested that some amount of force was required to induce rupture of emerin-treated nuclei. In our typical assay, nuclei in extract were pipetted onto a glass slide and overlaid with a glass coverslip for imaging. The force imparted by the coverslip was sufficient to rupture emerin-treated nuclei. On the other hand, if emerin was carefully added to a drop of extract on a glass coverslip, nuclear breakage was not immediately evident until the extract was mixed (Supplemental Video 1). To further address this issue, we utilized a microfluidic device that allowed nuclei in extract to be visualized immediately upon mixing with emerin. Time-lapse imaging of this mixing process clearly showed generation of elongated DNA strings after apparent nuclear rupture, and DNA aggregation frequently clogged the device (Supplemental Video 2). Emerin-induced nuclear breakage was also evident when nuclei in extract were encapsulated in droplets (Supplemental Figure S2D).

Rescue of emerin-induced nuclear breakage
To begin to address the mechanism of emerin-induced nuclear rupture, we tested whether nuclear localization of emerin was required. Nuclei were pretreated with wheat germ agglutinin (WGA) to occlude nuclear pore complexes and prevent nuclear import. WGA-treated nuclei still ruptured upon emerin addition, suggesting that breakage was not induced by intranuclear emerin (Supplemental Figure S3A). This prompted us to examine the localization of ectopically added emerin using a fluorescently tagged version of emerin that still retained the ability to induce nuclear rupture. We primarily observed small emerin puncta that colocalized with DiI-stained membrane, and in some cases we observed larger emerin aggregates that were also membrane-localized. Notably, we did not detect any emerin associated with in vitro–assembled nuclei (Figure 2A). Consistent with these data, the recombinant emerin LEM domain also did not localize to nuclei assembled in *Xenopus* egg extract (Dreger *et al.*, 2002). Because emerin is associated with cytoplasmic membrane and does not have to be intranuclear to induce breakage, we surmise that emerin is exerting its effect on nuclear integrity from outside the nucleus in the cytoplasm.

We next tested whether nuclear breakage could be rescued by altering emerin's localization. Emerin lacking its transmembrane domain (amino acids 228–242) did not induce nuclear rupture (Figure 3), nor did the LEM domain alone (Dreger *et al.*, 2002). Emerin
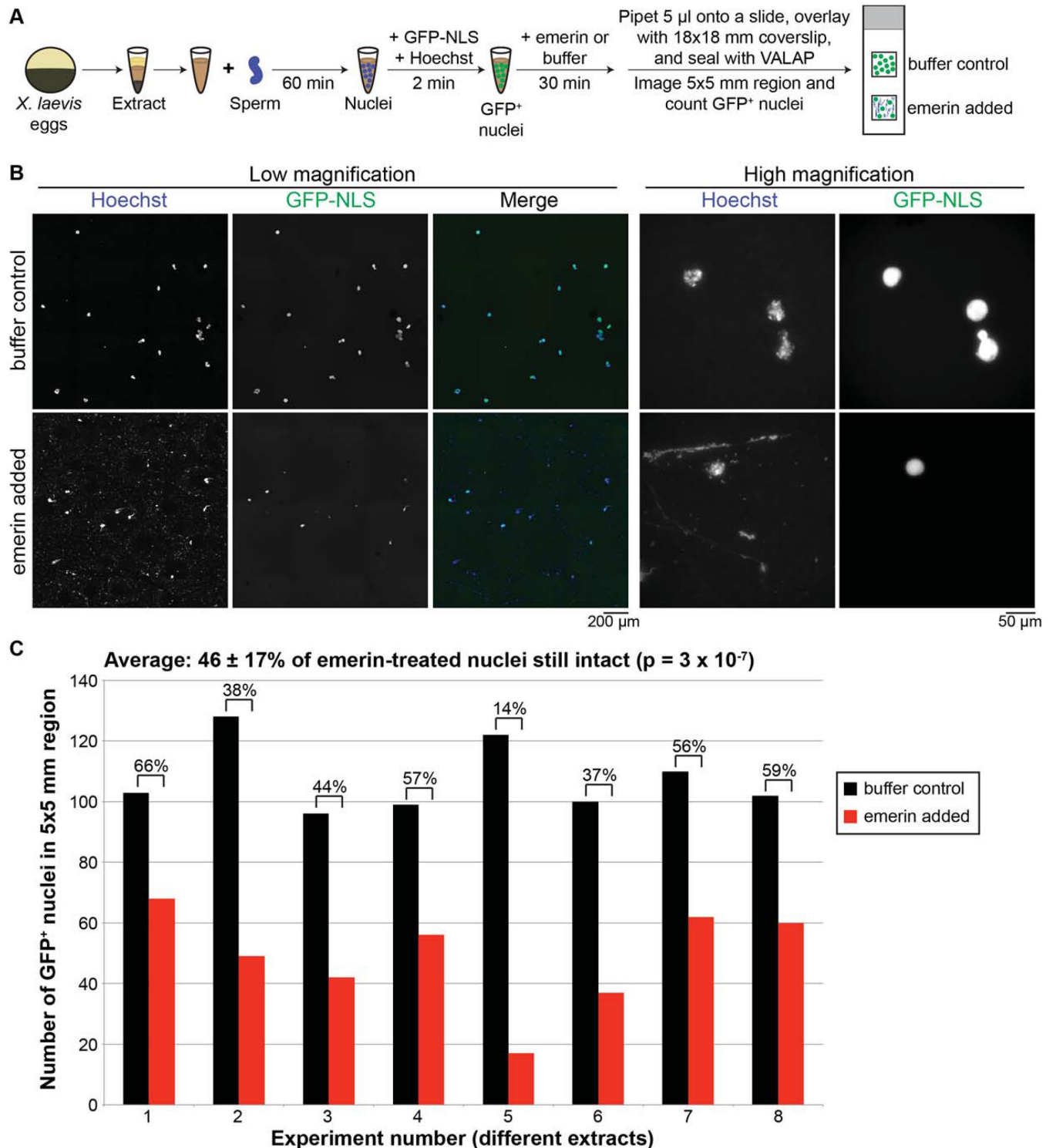
FIGURE 1: Emerin induces breakage of *X. laevis* egg extract nuclei. (A) Experimental approach. See *Materials and Methods* for further details. (B) Representative images of nuclei treated with dialysis buffer or 5 nM recombinant emerin. (C) Quantification of the nuclear breakage phenotype. The intact GFP+ nuclei were counted for buffer- or emerin-treated nuclei in eight different *X. laevis* egg extracts. Above each pair of bars is the percentage of intact emerin-treated nuclei compared with the buffer control. Above the graph is the average of all data.

purified in a complex with TRC40 (also known as ASNA1), a protein responsible for targeting emerin to the inner nuclear membrane (Yamamoto and Sakisaka, 2012; Pfaff *et al.*, 2016), was properly targeted to nuclei in extract (Figure 2B), and nuclear breakage was no longer observed (Figure 3). It is worth noting that TRC40 is up-regulated in *X. laevis* embryos only after the midblastula transition (MBT; Peshkin *et al.*, 2015). To test whether emerin has a deleterious effect on nuclei because its transmembrane domain is unchaperoned, we
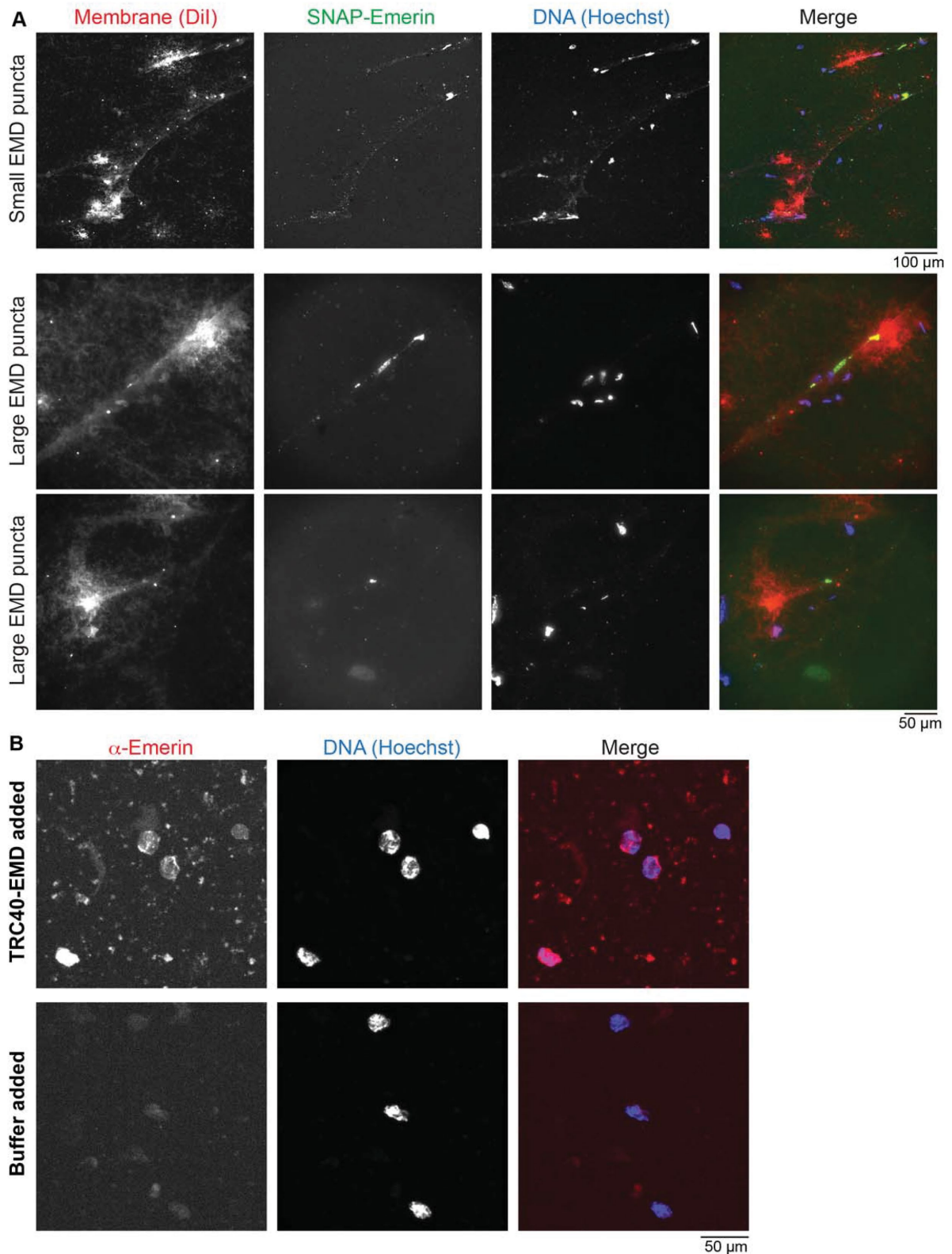
FIGURE 2: TRC40 rescues emerin's nuclear localization. (A) Experiments were performed as in Figure 1, except that the extract was supplemented with 1 µM DiI and 0.4 µM SNAP-emerin conjugated to Alexa Fluor 488. Representative images of small and large emerin puncta are shown. (B) Nuclei assembled in *X. laevis* egg extract as shown in Figure 1 were supplemented with 8 nM TRC40-EMD or an equivalent volume of dialysis buffer. After a 30-min incubation, nuclei were fixed, spun down onto coverslips, and stained with an anti-emerin antibody and Hoechst. Emerin images were acquired with the same exposure time. Representative images are shown.
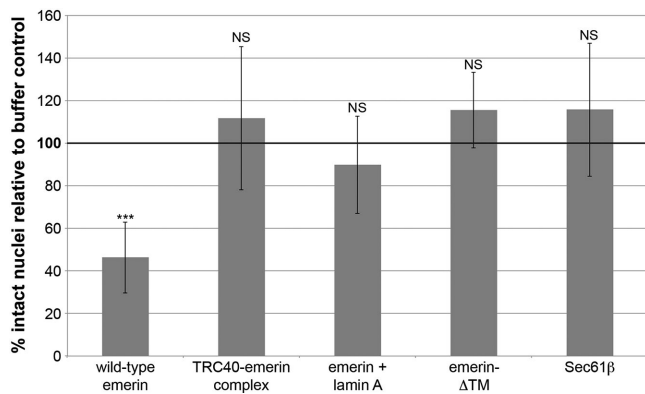
FIGURE 3: Rescue of nuclear breakage. Experiments and quantification were performed as in Figure 1. Data are plotted as the mean and SD from multiple independent experiments. The wild-type emerin data are the same as presented in Figure 1C ($n = 8$ extracts). TRC40-emerin was added at 5 nM ($n = 6$ extracts). For the "emerin + lamin A experiment," recombinant lamin A was added during nuclear assembly at 1 nM before the addition of 5 nM emerin ($n = 5$ extracts). The emerin-ΔTM protein (deletion of transmembrane domain amino acids 228–242) was added at 5 nM ($n = 4$ extracts). The Sec61β protein was added at 5 nM ($n = 2$ extracts), and 50 nM Sec61β also did not induce nuclear breakage (unpublished data). Across all experiments, the average number of intact nuclei for buffer controls was 240. Statistical analysis was performed relative to the buffer control, which was normalized to 100% intact nuclei (bold horizontal line). ***$p < 0.005$; NS, not significant.

tested a different unchaperoned tail-anchored membrane protein, Sec61β, finding that it failed to induce nuclear breakage (Figure 3). Consistent with emerin having an effect specific to nuclear integrity, emerin did not qualitatively disturb or alter nonnuclear membrane structures visualized with DiI (Supplemental Figure S3B).

We next preassembled nuclei with lamin A, an important emerin-interacting partner not present in egg extract (Wolin *et al.*, 1987; Gareiss *et al.*, 2005; Jevtic *et al.*, 2015), and found that these nuclei were resistant to emerin-induced breakage (Figure 3), possibly because lamin A increases NE stiffness (Lammerding *et al.*, 2006; Paje-rowski *et al.*, 2007; Neelam *et al.*, 2015; Stephens *et al.*, 2017). In addition, nuclei isolated from extract and resuspended in buffer failed to break upon exposure to emerin, showing that extract, and likely membrane within extract, is required for emerin-induced nuclear rupture (Supplemental Figure S3C). It is worth noting that when we added emerin to extract before nuclear assembly, we observed some emerin localized to the DNA (Supplemental Figure S3D) and some nuclei formed, albeit with altered nuclear shape (unpublished data). Thus, nuclear rupture can be rescued by incorporating emerin or lamin A into the NE or by disrupting emerin's membrane association.

Emerin induces nuclear breakage and inviability in *Xenopus* embryos

We next asked whether emerin would induce rupture of in vivo–assembled nuclei. Our first approach was to fertilize *Xenopus* eggs, allow them to develop to different embryonic stages, and then prepare embryo extracts containing endogenous embryonic nuclei. Nuclei in early-stage embryo extracts (stages 5–8) were susceptible to emerin-induced breakage, similar to what was observed with in vitro–assembled nuclei. Of interest, nuclei in later stages 10–11 remained intact upon emerin addition (Figure 4A). Because *Xenopus* nuclei scale smaller as development progresses, we wondered

whether emerin failed to induce rupture of these nuclei because of their smaller size. To test this idea, we assembled nuclei in egg extract but only allowed them to grow for a brief period of time, reaching an average cross-sectional area similar to that of stage 9–10 nuclei. These small egg extract nuclei still broke upon emerin addition (Figure 4B), indicating that susceptibility to nuclear breakage is likely not dictated by nuclear size.

Using a second approach, we microinjected fertilized one cell–stage embryos with recombinant emerin or dialysis buffer as a control. Buffer-injected embryos developed normally, while emerin-injected embryos began to show a loss of viability at stage 8, a time when cell motility is acquired in some regions of the embryo. The percentage of embryos that had ceased development increased at stage 10 and beyond, coinciding with gastrulation (Figure 5, A and B). While less than 20% of emerin-injected embryos reached stage 12 of development, more than 90% of embryos microinjected with the TRC40–emerin complex survived (unpublished data). Imaging of emerin-injected embryos revealed many apparently broken nuclei with a stringy DNA appearance similar to that observed for emerin-treated egg and embryo extract nuclei (Figure 5C).

To test whether emerin synthesized within the embryo would have a similar effect, we microinjected mRNA encoding emerin. As with protein microinjections, emerin mRNA induced a loss of embryo viability (Figure 6A and Supplemental Video 3). The effect was concentration–dependent, with 500, 1000, and 1500 pg of microinjected mRNA resulting in 64%, 25%, and 0% of embryos reaching stage 12, respectively (Figure 6B). To examine nuclear integrity in these embryos, we comicroinjected mRNA encoding GFP-NLS and emerin. Many cells in emerin-expressing embryos exhibited stringy DNA and a general loss of the nuclear GFP-NLS signal (Figure 6C). To quantify the latter effect, we isolated nuclei from microinjected embryos and counted the nuclei with intranuclear GFP-NLS. There was a more than 50% reduction in the number of GFP+ nuclei in emerin-expressing embryos (Figure 6D), suggesting that in vivo–produced emerin leads to a loss of nuclear integrity. We also microinjected embryos with mRNA encoding GFP-emerin. At stages 8 and 10, GFP-emerin often appeared punctate or diffusely cytoplasmic (Supplemental Figure S4), similar to what was observed in vitro (Figure 2A). This was particularly evident in cells with elongated, stringy DNA masses where nuclei had presumably ruptured (Supplemental Figure S4). Nuclear breakage and lysis in a subset of cells are likely sufficient to arrest development, leading to embryo inviability. A similar phenotype was observed in some stage 12 cells, while in other cells, GFP-emerin was properly localized to the nuclear periphery, as well as to the cytoplasm and cell cortex (Supplemental Figure S4). Taken together, these data show that cytoplasmic localization of emerin in early stage embryos is associated with nuclear rupture and embryo inviability.

DISCUSSION

We find that emerin added to *Xenopus* egg extract and early embryos is localized to the cytoplasm and induces nuclear breakage that can be rescued by disrupting emerin's membrane localization or by properly targeting emerin or lamin A to the nucleus. Why might emerin localized away from the nucleus induce nuclear rupture? One possibility is that cytoplasmic emerin sequesters other nuclear proteins, causing nuclei to become fragile and susceptible to breakage upon the application of force. This seems unlikely, given that nuclear breakage was observed after very brief incubation periods (Figure 4B, Supplemental Figure S1D, and Supplemental Video 1), and there was no evidence of nucleoporin or Man1 aggregates in the cytoplasm (Supplemental Figure S2, A–C).
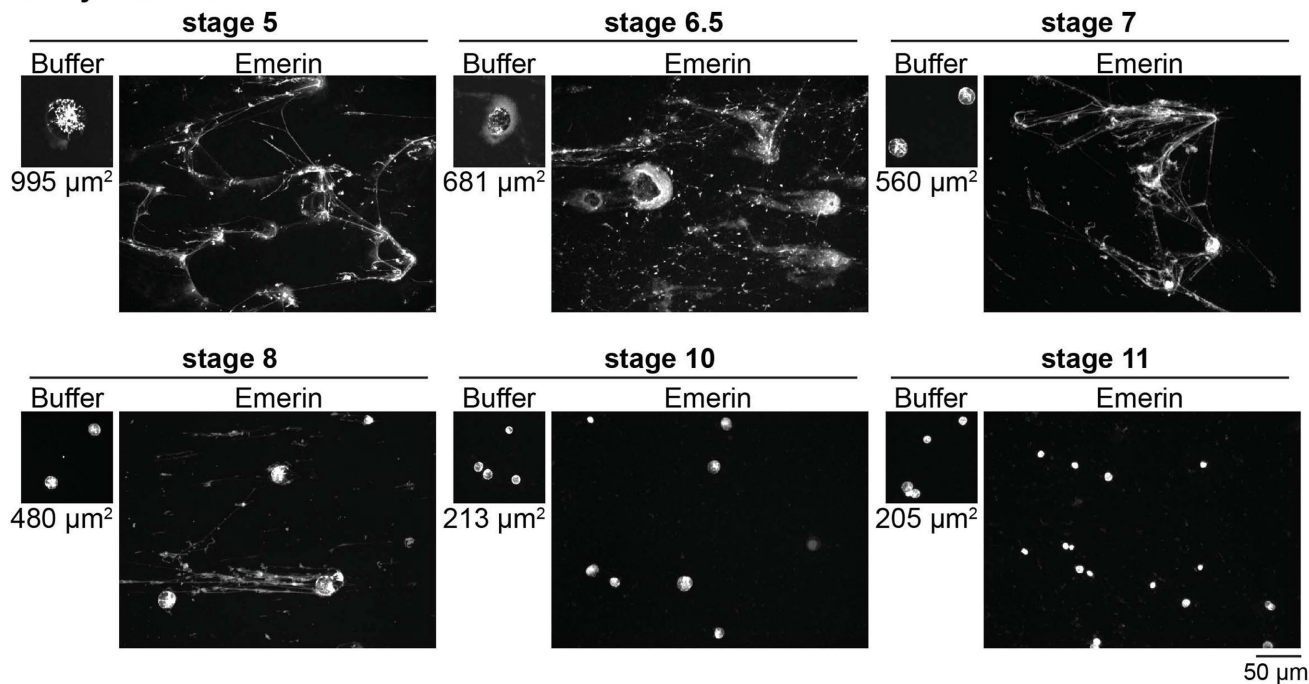
A Embryonic nuclei
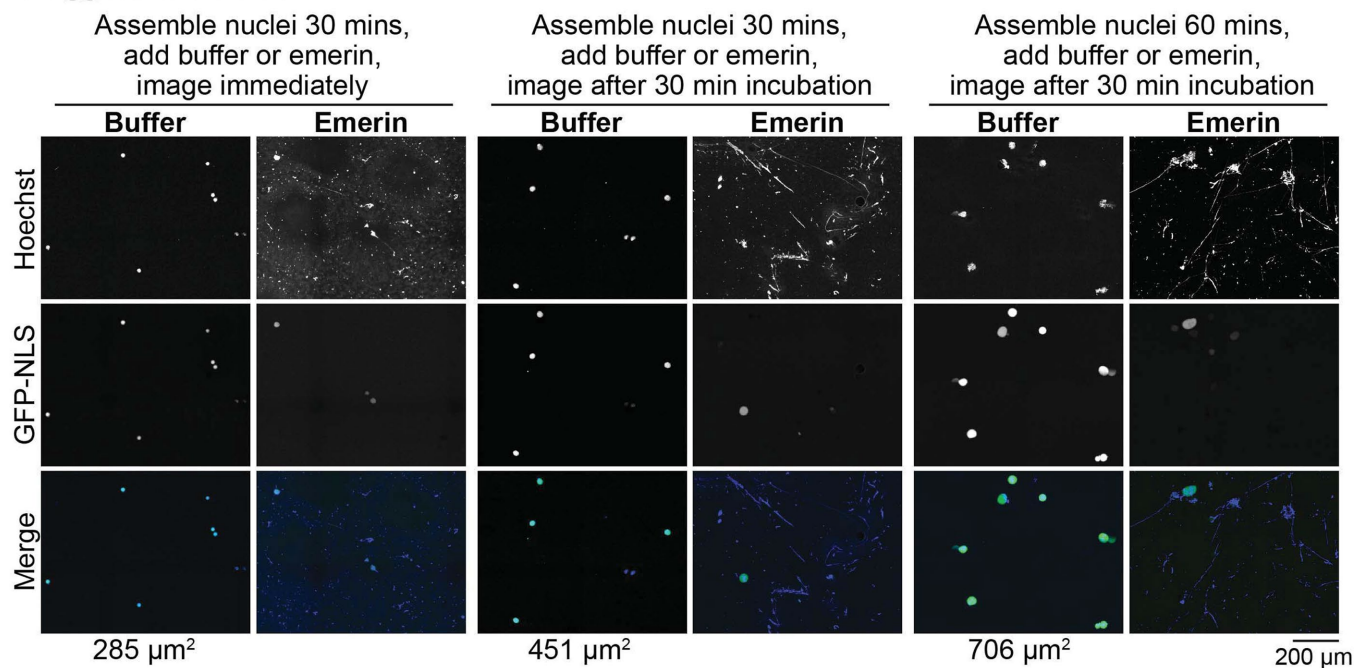
FIGURE 4: Early stage *X. laevis* embryonic nuclei are susceptible to emerin-induced breakage. (A) Embryo extracts containing endogenous embryonic nuclei were prepared from different-stage *X. laevis* embryos. At least 30 embryos were used per extract. Extracts were supplemented with 5 nM emerin or an equivalent volume of dialysis buffer as a control and incubated at room temperature for 30 min. Nuclei were stained with Hoechst and visualized as in Figure 1. Representative images from one experiment out of three are shown. Average nuclear cross-sectional area at each developmental stage is indicated in μm² (Jevtic and Levy, 2015). (B) Experiments were performed with *X. laevis* egg extract as in Figure 1, except that the lengths of nuclear assembly and emerin incubation were varied as indicated, so that the nuclei were different sizes when emerin was added. Representative images from one experiment out of three are shown. Average nuclear cross-sectional area for each condition is indicated in μm².

Another possibility is that emerin disrupts the incorporation of nucleoporin-containing annulate lamellae into the NE, a process that has been described in early *Drosophila* development (Hampoelz *et al.*, 2016) and likely also occurs in *Xenopus* given its vast maternal stores of annulate lamellae (Dabauvalle *et al.*, 1991; Cordes *et al.*, 1995; Beckhelling *et al.*, 2003). Arguing against this idea is the fact that intact emerin-treated nuclei exhibited continuous nucleoporin staining (Supplemental Figure S2, A and B), suggesting that the
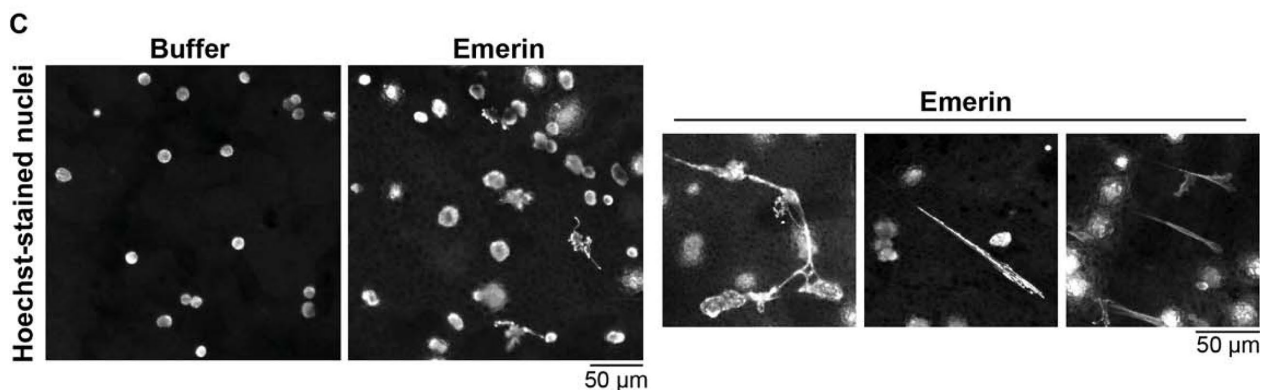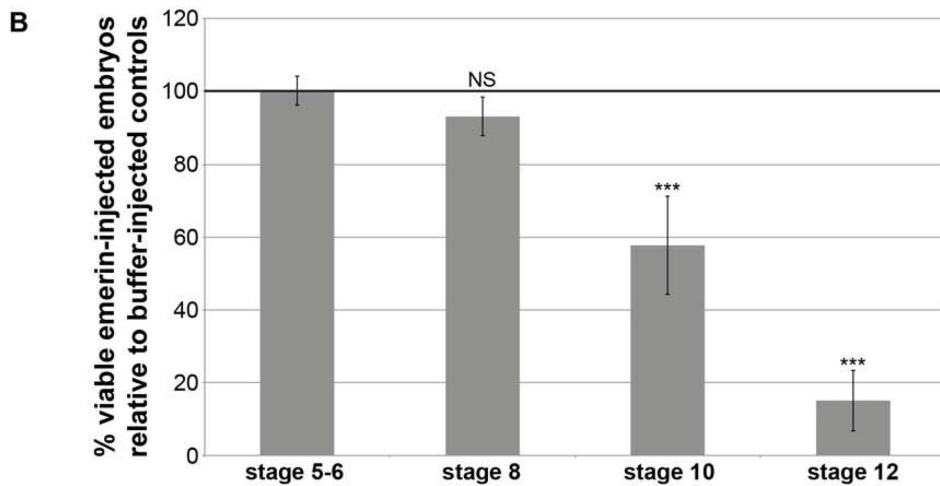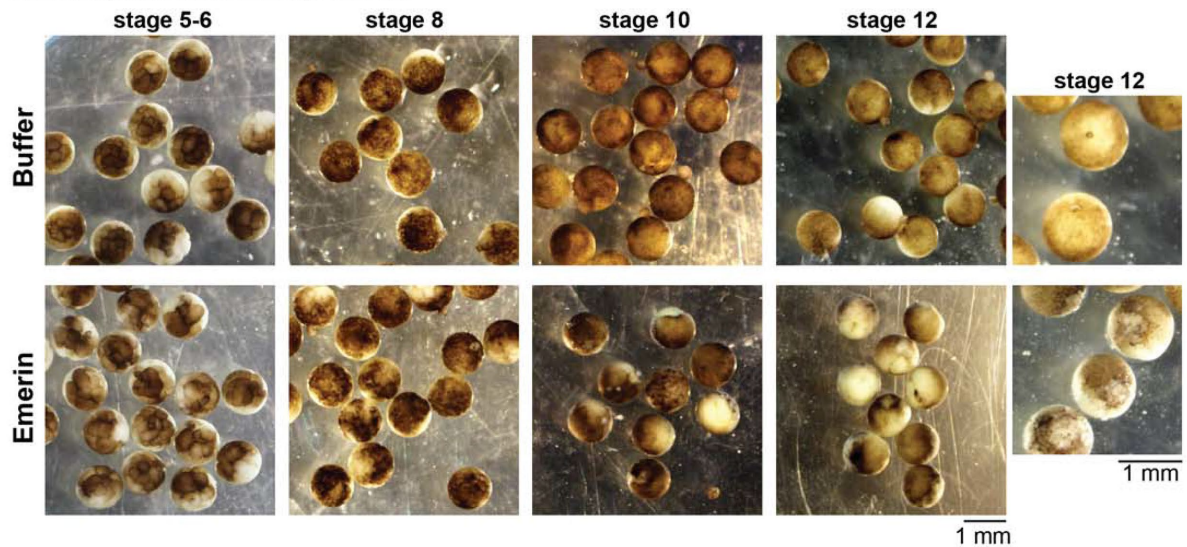
FIGURE 5: Microinjected emerin protein induces nuclear breakage and death in *X. laevis* embryos. (A) One-cell embryos were microinjected with emerin to achieve a final concentration of 0.5 nM within the embryo or an equivalent volume of dialysis buffer and allowed to develop at room temperature. Representative images at different developmental stages are shown. (B) At the indicated developmental stages, the viable embryos were counted. Inviable embryos were those that had stopped dividing or exhibited a puffy white appearance indicative of apoptosis (Johnson *et al.*, 2010; Du Pasquier *et al.*, 2011; Tokmakov *et al.*, 2011; Gillespie *et al.*, 2012; Willis *et al.*, 2012; Iguchi *et al.*, 2013; Broadus *et al.*, 2015). The number of viable embryos was normalized to the buffer control. From 30 to 60 embryos were analyzed per condition per experiment. Averages from three independent experiments are shown. Error bars represent SD. Statistical analysis was performed relative to the stage 5–6 embryos. ***$p < 0.005$; NS, not significant. (C) Nuclei in buffer- or emerin-microinjected embryos were visualized with Hoechst at stage 12. Representative images from one experiment out of three are shown.
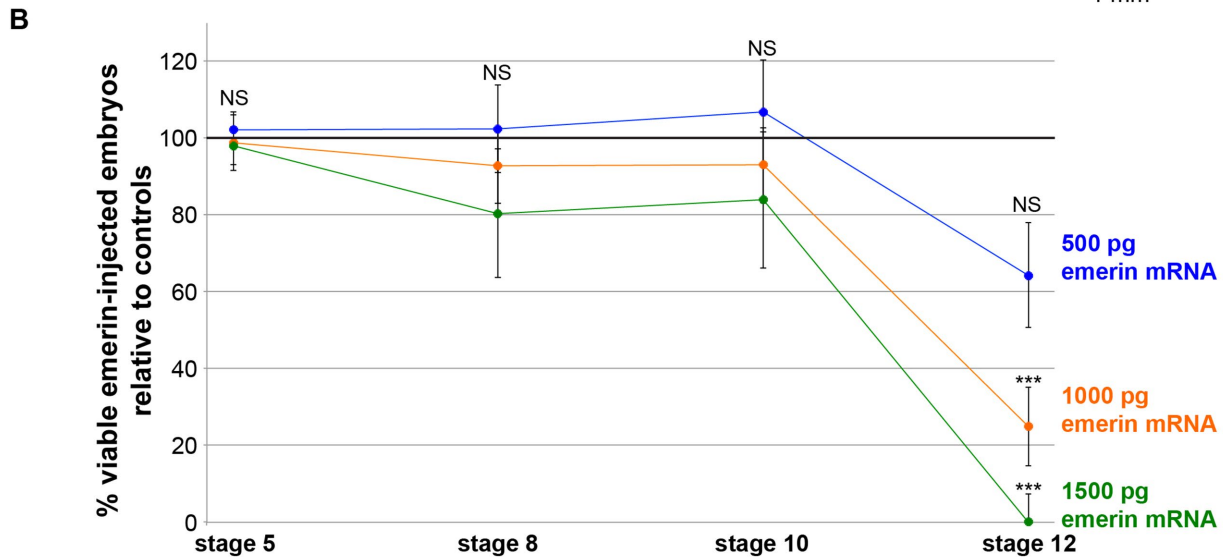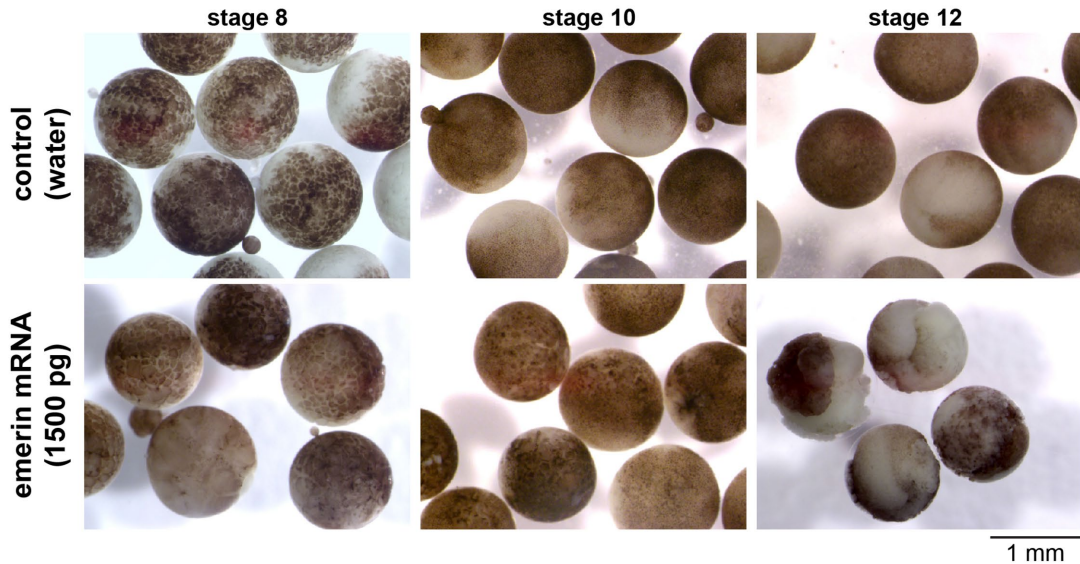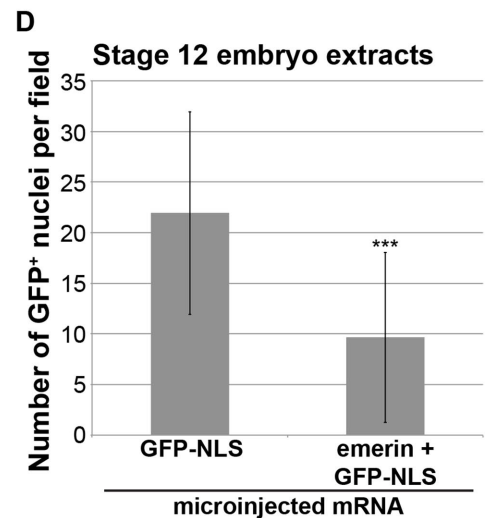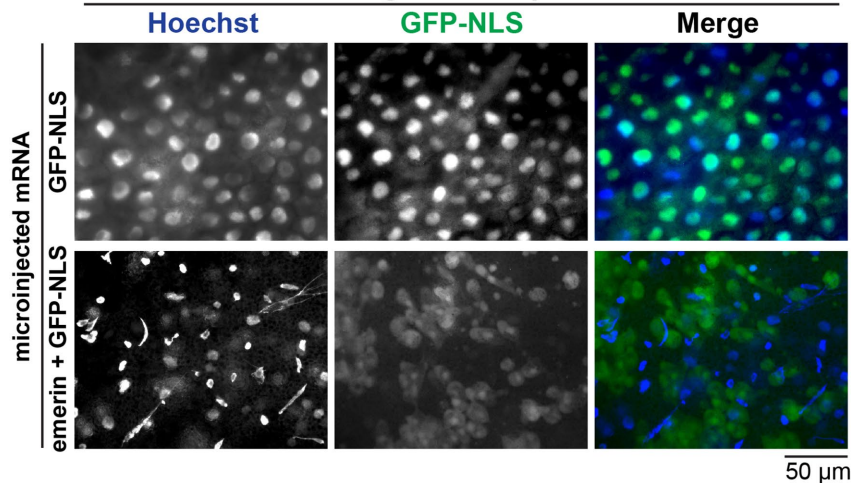
FIGURE 6: Microinjected emerin mRNA induces loss of nuclear integrity and death in *X. laevis* embryos. (A) One-cell embryos were microinjected with 1500 pg of emerin mRNA (dissolved in water) or an equivalent volume of water as a control and allowed to develop. Representative images at different developmental stages are shown. (B) One-cell embryos were microinjected with the indicated amounts of emerin mRNA or an equivalent volume of water as a control

permeability barrier of the NE remained intact. Another model is that egg extract nuclei are more susceptible to rupture, particularly when emerin is not properly integrated into the membrane, as in our heterologous system. In that scenario, adding lamin A or properly targeting emerin to the nucleus might generate a more rigid NE that is resistant to breakage (Lammerding *et al.*, 2006; Rowat *et al.*, 2006; Pajerowski *et al.*, 2007; Guilluy *et al.*, 2014; Neelam *et al.*, 2015; Stephens *et al.*, 2017). It is also possible that emerin–emerin interactions might aberrantly tether disparate membrane structures within the cytoplasm (Berk *et al.*, 2014; Herrada *et al.*, 2015; Samson *et al.*, 2017). Shear force applied to this network of interactions might lead to membrane tearing that propagates to the nucleus through ER–NE contacts, leading to nuclear breakage. Future work will address the mechanism of emerin-induced nuclear rupture.

While egg extract and early-stage embryonic nuclei rupture upon emerin addition, nuclei isolated from later-stage embryos are resistant to emerin-induced breakage, possibly because the biochemical composition of these nuclei has changed. Zygotic transcription is massively up-regulated at stage 8, coinciding with the MBT (Newport and Kirschner, 1982; Collart *et al.*, 2014). In particular, post-MBT embryos express lamin A (Wolin *et al.*, 1987; Gareiss *et al.*, 2005; Jevtic *et al.*, 2015) and up-regulate TRC40 transcription (Peshkin *et al.*, 2015), potentially explaining why post-MBT nuclei no longer rupture upon emerin addition. Consistent with this idea, GFP-emerin exhibited normal NE localization in some stage 12 cells (Supplemental Figure S4). While emerin induces rupture of early-stage embryonic nuclei, embryo death only manifests later in development, when cell motility and gastrulation movements may impart sufficient force for nuclear rupture (Chien *et al.*, 2015). It is also possible that nuclear rupture in emerin-injected embryos occurs before the onset of bulk MBT transcription, potentially explaining why emerin-injected embryos exhibit a post-MBT loss in viability while post-MBT nuclei isolated from uninjected embryos are resistant to emerin-induced breakage.

Because emerin is not normally present in *Xenopus* eggs and early-stage embryos, it is possible that ectopically added emerin is not present in its native state due to improper posttranslational modification or membrane insertion. Given the heterologous nature of this system, what might be the physiological relevance of our findings? First, the phenotype we observe is striking and suggests that emerin possesses an inherent ability to induce nuclear rupture, even if this activity is not evident in most cellular settings. Second, emerin is not expressed in early embryogenesis, and our results indicate that the presence of emerin would be deleterious for devel-

opment. This suggests that nuclei in early embryos possess unique structural and/or mechanical properties that change later in development when emerin is expressed. Regulated changes in nuclear structure/mechanics might be important for normal development; for instance, nuclear structure may be simplified in early development due to rapid cell divisions, and as a result these nuclei may be weaker and more susceptible to breakage. Such developmental changes in nuclear mechanics have been suggested in *Drosophila* (Hampoelz *et al.*, 2016). There is a growing literature on NE rupture and repair (Vargas *et al.*, 2012; Denais *et al.*, 2016; Raab *et al.*, 2016; Hatch, 2018), and our emerin findings might be relevant in nondevelopmental contexts where nuclei may be more deformable, for instance, in lamin-deficient cells, motile cancer cells, and certain immune cells (Sullivan *et al.*, 1999; Lammerding *et al.*, 2004, 2005; Denais and Lammerding, 2014; Denais *et al.*, 2016; Raab *et al.*, 2016). Consistent with this idea, we found that lamin A, which rigidifies the NE (Lammerding *et al.*, 2006; Pajerowski *et al.*, 2007; Neelam *et al.*, 2015; Stephens *et al.*, 2017), abrogated emerin-induced nuclear breakage. Third, while a cytoplasmic pool of emerin likely plays important roles in normal cells (Salpingidou *et al.*, 2007), emerin often exhibits a shift toward the endoplasmic reticulum in EDMD, as well as in some laminopathies caused by mutated lamin A (Ellis *et al.*, 1998; Fairley *et al.*, 1999, 2002). Perhaps, when emerin's distribution between the nucleus and cytoplasm is altered, nuclear and ER stability are impacted and emerin's nuclear rupturing activity becomes physiologically relevant, potentially contributing to disease. We can speculate that EDMD disease phenotypes manifest in muscle cells because these cells experience forces capable of disrupting nuclear structure. Changes in NE protein expression levels and localizations are also frequently observed in cancers (Chow *et al.*, 2012; Denais and Lammerding, 2014; Jevtic and Levy, 2014). Finally, given the surprising impact that emerin can have on nuclear structure and embryo viability, new therapeutic strategies might involve altering the localization of NE structural proteins.

MATERIALS AND METHODS
Plasmids
The human emerin gene was cloned into pDEST17 using the Gateway LR Clonase II kit (ThermoFisher 11791-020) and donor plasmid HsCD00081619 (DNASU) to generate pDL87. The SNAP tag was amplified from pSNAP (T7)-2 (NEB) by PCR and cloned into pET30a at *Nco*I and *Sac*I to generate pDL96. Human emerin was amplified from pDL87 by PCR and cloned into pDL96 at *Sal*I and *Not*I to generate SNAP-emerin pET30a (pDL97). The TRC40-EMD expression plasmid

and allowed to develop. At the indicated developmental stages, the viable embryos were counted. Inviable embryos were those that had stopped dividing or exhibited a puffy white appearance indicative of apoptosis (Johnson *et al.*, 2010; Du Pasquier *et al.*, 2011; Tokmakov *et al.*, 2011; Gillespie *et al.*, 2012; Willis *et al.*, 2012; Iguchi *et al.*, 2013; Broadus *et al.*, 2015). The number of viable embryos was normalized to water-microinjected controls. From 11 to 89 embryos were analyzed per condition per experiment (43 embryos on the average). Averages from three independent experiments are shown. Error bars represent SD. Statistical analysis was performed relative to the water-microinjected control embryos. ***$p < 0.005$; NS, not significant. Injection with 100 pg emerin mRNA had no effect on embryo viability, and 2000 pg emerin mRNA exerted an effect similar to 1500 pg (unpublished data). (C) One-cell embryos were microinjected with 1000 pg GFP-NLS mRNA with or without 1500 pg emerin mRNA and allowed to develop. When control embryos reached stage 12, nuclei in microinjected embryos were visualized with Hoechst and GFP-NLS. Representative images from one experiment out of two are shown. (D) When control embryos reached stage 12, extracts were prepared from equivalent numbers of microinjected embryos described in C. Equivalent volumes of extract were supplemented with Hoechst, applied to a slide, overlaid with a coverslip, and incubated for 15 min. Images were acquired and the intact GFP+ nuclei per ~660 × 660 µm field were counted. Nuclei from at least six fields were counted per experiment and condition. Averages from two independent experiments are shown. Error bars represent SD. ***$p < 0.005$.

was a gift from Ralph Kehlenbach (Georg-August-Universität, Göttingen, Germany; Pfaff *et al.*, 2016). The transmembrane domain of emerin (amino acids 228–242) was deleted from pDL87 using site-directed mutagenesis to generate pDL104 (Berk *et al.*, 2014). The fragment corresponding to EGFP-FLAG-cGAS was removed from Addgene plasmid #86675 (pTRIP-CMV-GFP-FLAG-cGAS; Raab *et al.*, 2016) with *Kpn*I/*Sal*I and cloned into pRSETA at *Kpn*I/*Xho*I to generate pRSETA EGFP-FLAG-cGAS (pDL105). Human emerin was amplified from pDL87 by PCR and cloned at *Bam*HI/*Xho*I into a pET30b vector containing the GFP sequence at *Eco*RV/*Bam*HI to produce a GFP–emerin fusion (pDL98). The *Bam*HI/*Xho*I fragment from pDL98 was ligated into pCS2+ to generate emerin pCS2+ (pDL113). The *Eco*RV/*Xho*I fragment from pDL98 was ligated into pCS2+ to generate GFP-emerin pCS2+ (pDL114). The GFP-NLS pCS2+ plasmid (pDL20) was described previously (Edens and Levy, 2014). The H2B-RFP pCS107 plasmid (pRH199) was a gift from Rebecca Heald (University of California, Berkeley).

Proteins
For emerin expression and purification, pDL87, pDL97, and pDL104 were transformed into BL21(DE3)RIL+ cells (Agilent). Cultures (1 l) were grown at 37°C to $OD_{600\ nm}$ 0.5–0.7 and induced with 1 mM isopropyl β-D-1-thiogalactopyranoside at 37°C for 4 h, or in some cases overnight. Cells were harvested and stored at –80°C. Cell pellets were thawed on ice, resuspended in 40 ml cell lysis buffer (100 mM NaH_2PO_4, 10 mM Tris-Cl, 150 mM NaCl, 1 mM dithiothreitol, 10 µg/ml leupeptin, 10 µg/ml pepstatin, 10 µg/ml chymostatin, 1 mM phenylmethylsulfonyl fluoride, Sigma S8830 protease inhibitor tablet, 1.9 mg/ml lysozyme, pH 6.0), and incubated on ice for 15 min. Cell lysates were subjected to sonication (Branson, 20% power, 4 min total, 10 s on/20 s off cycles). Lysates were centrifuged at 15,000 rpm in a JA-20 rotor for 15 min at 4°C. The supernatant was discarded, and pellets were resuspended in 20 ml cell lysis buffer supplemented with 1% Triton X-100. After another round of centrifugation, the supernatant was again discarded and pellets were resuspended in 20 ml denaturation buffer (100 mM NaH_2PO_4, 10 mM Tris-Cl, 8 M urea, 3 mM 2-mercaptoethanol, pH 8.0) using a Dounce homogenizer. After another round of centrifugation, the supernatant was collected and dialyzed against dialysis buffer (10 mM HEPES, 300 mM KCl, 50 mM sucrose, 5% glycerol, pH 7.8) using Slide-A-Lyzer dialysis cassettes (10,000 MWCO, Thermo 66380) at 4°C. The first round of dialysis was with 1 l of dialysis buffer for 4 h, followed by a second round of dialysis using another 1 l of dialysis buffer overnight. Protein aliquots were stored at –80°C. To approximate protein concentrations, emerin stock solutions and BSA standards were separated on SDS–PAGE gels and stained with Coomassie. Band intensities were measured using ImageStudio (Li-Cor). In some cases the denaturation buffer was supplemented with 10 mM deoxycholic acid and the dialysis buffer consisted of 50 mM Tris-Cl (pH 8), 150 mM KCl, 5% glycerol, and 10 mM deoxycholic acid. In other instances, dialyzed emerin was subjected to Ni-NTA affinity chromatography and an additional round of dialysis. Emerin purified using each of these different schemes induced similar frequencies of nuclear breakage in extract. SNAP-emerin generated from pDL97 was labeled with Janelia Fluor 549 (Grimm *et al.*, 2015) or Alexa Fluor 488 according to the manufacturer's protocol (S9129, NEB). The TRC40-EMD complex was purified as previously described (Pfaff *et al.*, 2016). GST-GFP-NLS (pMD49) was purified as previously described (Levy and Heald, 2010). Lamin A was expressed and purified from pDL36 as previously described (Jevtic *et al.*, 2015). EGFP-cGAS was expressed from pDL105 and purified by Ni-NTA affinity chromatography as

previously described (Kranzusch *et al.*, 2013). Recombinant human Sec61β protein was obtained from Abcam (ab161213).

Western blots
Western blots were performed as previously described (Vukovic *et al.*, 2016). The primary antibody against emerin (MANEM1 5D10; Wolfson Centre for Inherited Diseases) was used at 1:100. IRDye 680RD anti-mouse (Li-Cor 925-68070) secondary antibody was used at 1:20,000. Blots were scanned on a Li-Cor Odyssey CLx instrument, and band quantification was performed with ImageStudio.

Xenopus egg extract experiments
In vitro nuclear assembly using *X. laevis* egg extract and demembranated *X. laevis* sperm nuclei was performed as previously described (Edens and Levy, 2014; Chen and Levy, 2018). Briefly, reactions consisted of 100–500 µl of metaphase-arrested egg extract supplemented with energy mix, 0.15 mg/ml cycloheximide, 0.5 mM $CaCl_2$, and demembranated *X. laevis* sperm nuclei at 1000/µl. After 1 h of nuclear assembly at room temperature, nuclear functionality was assessed by adding 40 µg/ml recombinant GST-GFP-NLS and confirming its nuclear import. Hoechst was added at 10 µg/ml to visualize the DNA. To preassembled nuclei, varying concentrations of recombinant emerin protein were then added (not to exceed 10% of the reaction volume). Unless otherwise noted, the usual final concentration of emerin added was 5 nM. Control reactions were supplemented with equal volumes of dialysis buffer. After a 30-min incubation at room temperature, 5 µl of each reaction was pipetted onto a glass slide, overlaid with an 18 × 18 mm square coverslip, sealed with Valap (equal parts petroleum jelly, lanolin, and paraffin), and imaged immediately. Nuclear breakage was assessed by loss of nuclear GFP-NLS signal and/or the appearance of stringy/punctate Hoechst-stained DNA. For some experiments, nuclei were preassembled with 1 nM recombinant lamin A protein before addition of emerin or dialysis buffer. Where indicated, extract was supplemented with 0.2 mg/ml WGA (Sigma L9640) or 1 µM lipophilic dye CM-DiI (ThermoFisher C7001). To test the effect of emerin on smaller egg extract nuclei, the assay was performed in the same way, except that nuclear assembly and growth were allowed to proceed for only 30 min before addition of emerin or dialysis buffer. Where indicated, spindowns were performed as previously described: nuclei were fixed, spun down onto coverslips, and processed for immunofluorescence (Edens and Levy, 2014, 2016). Primary antibodies used for spindowns included α-emerin (mouse; MANEM1 5D10; Wolfson Centre for Inherited Diseases; 1:50), mAb414 (mouse; BioLegend #902901; 1:1000), and α-Man1 (rabbit; ThermoFisher Scientific #PA5-72734; 1:100). Secondary antibodies were used at 1:1000 and included Alexa Fluor 568 conjugated anti-mouse immunoglobulin G (IgG) and Alexa Fluor 488 conjugated anti-rabbit IgG. Where indicated, nuclei in extract were incubated for 10 min with 10 µg/ml mAb414 conjugated to Alexa Fluor 594 (BioLegend #682202). All *Xenopus* procedures and studies were conducted in compliance with the U.S. Department of Health and Human Services Guide for the Care and Use of Laboratory Animals. Protocols were approved by the University of Wyoming Institutional Animal Care and Use Committee (Assurance #A-3216-01).

Xenopus embryo experiments
X. laevis embryos and embryo extracts were prepared as previously described (Edens and Levy, 2014, 2016). Different-stage embryo extracts containing endogenous embryonic nuclei were supplemented with recombinant emerin protein or dialysis buffer. Nuclear breakage was assessed by appearance of stringy/punctate Hoechst-stained

DNA. Embryo microinjection was performed as previously described (Jevtic and Levy, 2015). Recombinant proteins were microinjected at the one-cell stage. Microinjection volumes were 10 nl, and emerin stock concentrations were adjusted so that the final concentration in the embryo was ~0.5 nM. Control embryos were microinjected with equal volumes of dialysis buffer. Emerin, GFP-emerin, GFP-NLS, and H2B-RFP mRNA were synthesized from pDL113, pDL114, pDL20, and pRH199, respectively, by first linearizing the plasmids with NotI and then expressing the mRNA from the SP6 promoter using the mMessage mMachine kit (Ambion). Purified mRNAs were resuspended in water. One-cell embryos were microinjected with 10 nl of mRNA, and the stock concentrations were adjusted to vary the amount of mRNA delivered. Water microinjections were used as a control. Embryos were allowed to develop to different stages, and embryos that stopped cleaving or appeared white and puffy were scored as apoptotic/inviable (Johnson et al., 2010; Du Pasquier et al., 2011; Tokmakov et al., 2011; Gillespie et al., 2012; Willis et al., 2012; Iguchi et al., 2013; Broadus et al., 2015). To visualize nuclei in microinjected embryos, single embryos were placed on a glass slide with 5 µl nuclear fix solution (Chen and Levy, 2018) and squashed under a coverslip.

Microscopy and image quantification
Wide-field microscopy was performed using an Olympus BX63 upright wide-field epifluorescence microscope. This system is equipped to perform multimode time-lapse imaging using an X-Cite 120LED illumination system. Image acquisition was with a high-resolution Hamamatsu ORCA-Flash4.0 digital CMOS camera at room temperature. Objectives included the UPLFLN20X and UPLSAPO40XS (Olympus). X–Y and Z positions were controlled by a fully motorized Olympus stage. Acquisition and automation were controlled by Olympus cellSens imaging software, and image analysis was performed using Metamorph software. Images for measuring fluorescence intensity were acquired using the same exposure times. For publication, images were cropped using ImageJ, but were otherwise unaltered. To quantify the number of intact nuclei with intranuclear GFP-NLS signal, 25- or 100-mm^2 images were acquired by image stitching using a UPLFLN20X objective (Olympus). Images were analyzed using Stream View (Olympus), and intact nuclei were counted over the entire scan area. Intact nuclei were identified as being both GFP$^+$ and Hoechst$^+$. Embryo images and movies were acquired with an Olympus SZX16 research fluorescence stereomicroscope, equipped with Olympus DP72 camera, 11.5× zoom microscope body, and SDFPLAPO1XPF objective. Where indicated, confocal imaging was performed on a spinning-disk confocal microscope based on an Olympus IX71 microscope stand equipped with a five-line LMM5 laser launch (Spectral Applied Research) and switchable two-fiber output to facilitate imaging through either a Yokogawa CSU-X1 spinning-disk head or a TIRF illuminator. Confocal images were acquired with an EM-CCD camera (ImagEM; Hamamatsu). Z-axis focus was controlled using a piezo Pi-Foc (Physik Instrumente), and multiposition imaging was achieved using a motorized Ludl stage. An Olympus UPLFLN 40× (NA 0.75, air) objective was used. Image acquisition and all system components were controlled using Metamorph software.

Microfluidic design, fabrication, and operation
Microfluidic devices were designed to expose flowing nuclei to and incubate them within an emerin solution via the hydrodynamic focusing of discrete, coflowing inlet streams (Knight et al., 1998; Kauffmann et al., 2001; Stiles et al., 2005). To generate slow, steady flows in which nuclei could be imaged during elongation, fluids were passively pumped using a combination of degassed poly(dimethylsiloxane) (PDMS) initial filling, permeation-driven flow, and hydrostatic pressure at each fluid inlet (Zhou et al., 2007; Gnyawali et al., 2017; Komeya et al., 2017). Hydrodynamic-focusing microfluidic devices were designed to include three inlet reservoirs feeding channels that merge at a cross-junction and flow to a large, high–surface area fluid reservoir with a single outlet. Devices were fabricated via well-documented soft lithography replication protocols (Xia and Whitesides, 1998). Briefly, a 50-µm layer of negative photoresist (SU8 50; MicroChem, Westborough, MA) was spin-coated upon a 100-mm silicon wafer and patterned by exposure to 365-nm UV light through a shadow mask (CAD/ART Services, Bandon, OR). Following a developer soak to dissolve unexposed resist, photoresist-on-silicon masters were buried in PDMS, degassed, and baked for 4 h at 70°C to cure them. Individual devices were cut and trimmed from the PDMS slab, inlet/outlet holes were punched, and the devices were bonded to a cover slip. Prior to filling, devices were placed in a vacuum chamber under house vacuum for ~1 h and removed, and each inlet reservoir was filled with an aliquot of XB buffer (100 mM KCl, 0.1 mM $CaCl_2$, 1 mM $MgCl_2$, 50 mM sucrose, 10 mM HEPES-KOH, pH 7.8). The flux of air from channels into the degassed PDMS matrix filled the channel network in a rapid, bubble-free manner. After initial device filling, excess buffer was removed from the inlets by dabbing with a Kimwipe, and each process fluid (emerin or in vitro–assembled nuclei in egg extract) was introduced to its respective inlet reservoir by the insertion of filled Tygon tubing. Nuclei in extract were labeled by adding Sytox Green at 1:1000 (Life Technologies; S7020, 5 mM stock). Flow was maintained by the continued permeation of fluid into the PDMS matrix and balanced by hydrostatic pressure achieved by controlling the height of each fluid in the tubing.

Statistics
Averaging and statistical analysis were performed for independently repeated experiments. Two-tailed Student's t tests assuming equal variances were performed in Excel (Microsoft) to evaluate statistical significance. The p values, numbers of independent experiments, and error bars are given in the figure legends.

REFERENCES
Barton LJ, Soshnev AA, Geyer PK (2015). Networking in the nucleus: a spotlight on LEM-domain proteins. Curr Opin Cell Biol 34, 1–8.

Beckhelling C, Chang P, Chevalier S, Ford C, Houliston E (2003). Pre-M phase-promoting factor associates with annulate lamellae in Xenopus oocytes and egg extracts. Mol Biol Cell 14, 1125–1137.

Bengtsson L, Wilson KL (2006). Barrier-to-autointegration factor phosphorylation on Ser-4 regulates emerin binding to lamin A in vitro and emerin localization in vivo. Mol Biol Cell 17, 1154–1163.

Berk JM, Simon DN, Jenkins-Houk CR, Westerbeck JW, Gronning-Wang LM, Carlson CR, Wilson KL (2014). The molecular basis of emerin-emerin and emerin-BAF interactions. J Cell Sci 127, 3956–3969.

Berk JM, Tifft KE, Wilson KL (2013). The nuclear envelope LEM-domain protein emerin. Nucleus 4, 298–314.

Bione S, Maestrini E, Rivella S, Mancini M, Regis S, Romeo G, Toniolo D (1994). Identification of a novel X-linked gene responsible for Emery-Dreifuss muscular dystrophy. Nat Genet 8, 323–327.

Broadus MR, Yew PR, Hann SR, Lee E (2015). Small-molecule high-through-put screening utilizing *Xenopus* egg extract. Methods Mol Biol 1263, 63–73.

Burke B, Stewart CL (2014). Functional architecture of the cell's nucleus in development, aging, disease. Curr Top Dev Biol 109, 1–52.

Chang W, Folker ES, Worman HJ, Gundersen GG (2013). Emerin organizes actin flow for nuclear movement and centrosome orientation in migrating fibroblasts. Mol Biol Cell 24, 3869–3880.

Chen P, Levy DL (2018). Nucleus assembly and import in *Xenopus laevis* egg extract. Cold Spring Harb Protoc, doi: 10.1101/pdb.prot097196.

Chien YH, Keller R, Kintner C, Shook DR (2015). Mechanical strain determines the axis of planar polarity in ciliated epithelia. Curr Biol 25, 2774–2784.

Chow KH, Factor RE, Ullman KS (2012). The nuclear envelope environment and its cancer connections. Nat Rev Cancer 12, 196–209.

Collart C, Owens ND, Bhaw-Rosun L, Cooper B, De Domenico E, Patrushev I, Sesay AK, Smith JN, Smith JC, Gilchrist MJ (2014). High-resolution analysis of gene activity during the *Xenopus* mid-blastula transition. Development 141, 1927–1939.

Cordes VC, Reidenbach S, Franke WW (1995). High content of a nuclear pore complex protein in cytoplasmic annulate lamellae of *Xenopus* oocytes. Eur J Cell Biol 68, 240–255.

Dabauvalle MC, Loos K, Merkert H, Scheer U (1991). Spontaneous assembly of pore complex-containing membranes ("annulate lamellae") in *Xenopus* egg extract in the absence of chromatin. J Cell Biol 112, 1073–1082.

Davidson PM, Lammerding J (2014). Broken nuclei—lamins, nuclear mechanics, disease. Trends Cell Biol 24, 247–256.

Demmerle J, Koch AJ, Holaska JM (2012). The nuclear envelope protein emerin binds directly to histone deacetylase 3 (HDAC3) and activates HDAC3 activity. J Biol Chem 287, 22080–22088.

Denais C, Lammerding J (2014). Nuclear mechanics in cancer. Adv Exp Med Biol 773, 435–470.

Denais CM, Gilbert RM, Isermann P, McGregor AL, te Lindert M, Weigelin B, Davidson PM, Friedl P, Wolf K, Lammerding J (2016). Nuclear envelope rupture and repair during cancer cell migration. Science 352, 353–358.

Dreger CK, Konig AR, Spring H, Lichter P, Herrmann H (2002). Investigation of nuclear architecture with a domain-presenting expression system. J Struct Biol 140, 100–115.

Du Pasquier D, Dupre A, Jessus C (2011). Unfertilized *Xenopus* eggs die by Bad-dependent apoptosis under the control of Cdk1 and JNK. PLoS One 6, e23672.

Edens LJ, Levy DL (2014). cPKC regulates interphase nuclear size during *Xenopus* development. J Cell Biol 206, 473–483.

Edens LJ, Levy DL (2016). A cell-free assay using *Xenopus laevis* embryo extracts to study mechanisms of nuclear size regulation. J Vis Exp 2016, doi: 10.3791/54173.

Ellis JA, Craxton M, Yates JR, Kendrick-Jones J (1998). Aberrant intracellular targeting and cell cycle-dependent phosphorylation of emerin contribute to the Emery-Dreifuss muscular dystrophy phenotype. J Cell Sci 111(Pt 6), 781–792.

Fairley EA, Kendrick-Jones J, Ellis JA (1999). The Emery-Dreifuss muscular dystrophy phenotype arises from aberrant targeting and binding of emerin at the inner nuclear membrane. J Cell Sci 112 (Pt 15), 2571–2582.

Fairley EA, Riddell A, Ellis JA, Kendrick-Jones J (2002). The cell cycle dependent mislocalisation of emerin may contribute to the Emery-Dreifuss muscular dystrophy phenotype. J Cell Sci 115, 341–354.

Gareiss M, Eberhardt K, Kruger E, Kandert S, Bohm C, Zentgraf H, Muller CR, Dabauvalle MC (2005). Emerin expression in early development of Xenopus laevis. Eur J Cell Biol 84, 295–309.

Gillespie PJ, Gambus A, Blow JJ (2012). Preparation and use of *Xenopus* egg extracts to study DNA replication and chromatin associated proteins. Methods 57, 203–213.

Gnyawali V, Saremi M, Kolios MC, Tsai SSH (2017). Stable microfluidic flow focusing using hydrostatics. Biomicrofluidics 11, 034104.

Grimm JB, English BP, Chen J, Slaughter JP, Zhang Z, Revyakin A, Patel R, Macklin JJ, Normanno D, Singer RH, *et al.* (2015). A general method to improve fluorophores for live-cell and single-molecule microscopy. Nat Methods 12, 244–250, 3 p following 250.

Gruenbaum Y, Margalit A, Goldman RD, Shumaker DK, Wilson KL (2005). The nuclear lamina comes of age. Nat Rev Mol Cell Biol 6, 21–31.

Guilluy C, Osborne LD, Van Landeghem L, Sharek L, Superfine R, Garcia-Mata R, Burridge K (2014). Isolated nuclei adapt to force and reveal a mechanotransduction pathway in the nucleus. Nat Cell Biol 16, 376–381.

Hampoelz B, Mackmull MT, Machado P, Ronchi P, Bui KH, Schieber N, Santarella-Mellwig R, Necakov A, Andres-Pons A, Philippe JM, *et al.* (2016). Pre-assembled nuclear pores insert into the nuclear envelope during early development. Cell 166, 664–678.

Haque F, Mazzeo D, Patel JT, Smallwood DT, Ellis JA, Shanahan CM, Shackleton S (2010). Mammalian SUN protein interaction networks at the inner nuclear membrane and their role in laminopathy disease processes. J Biol Chem 285, 3487–3498.

Haraguchi T, Holaska JM, Yamane M, Koujin T, Hashiguchi N, Mori C, Wilson KL, Hiraoka Y (2004). Emerin binding to Btf, a death-promoting transcriptional repressor, is disrupted by a missense mutation that causes Emery-Dreifuss muscular dystrophy. Eur J Biochem 271, 1035–1045.

Haraguchi T, Koujin T, Segura-Totten M, Lee KK, Matsuoka Y, Yoneda Y, Wilson KL, Hiraoka Y (2001). BAF is required for emerin assembly into the reforming nuclear envelope. J Cell Sci 114, 4575–4585.

Hatch EM (2018). Nuclear envelope rupture: little holes, big openings. Curr Opin Cell Biol 52, 66–72.

Helbling-Leclerc A, Bonne G, Schwartz K (2002). Emery-Dreifuss muscular dystrophy. Eur J Hum Genet 10, 157–161.

Herrada I, Samson C, Velours C, Renault L, Ostlund C, Chervy P, Puchkov D, Worman HJ, Buendia B, Zinn-Justin S (2015). Muscular dystrophy mutations impair the nuclear envelope emerin self-assembly properties. ACS Chem Biol 10, 2733–2742.

Hirano Y, Segawa M, Ouchi FS, Yamakawa Y, Furukawa K, Takeyasu K, Horigome T (2005). Dissociation of emerin from barrier-to-autointegration factor is regulated through mitotic phosphorylation of emerin in a *Xenopus* egg cell-free system. J Biol Chem 280, 39925–39933.

Ho CY, Jaalouk DE, Vartiainen MK, Lammerding J (2013). Lamin A/C and emerin regulate MKL1-SRF activity by modulating actin dynamics. Nature 497, 507–511.

Holaska JM, Kowalski AK, Wilson KL (2004). Emerin caps the pointed end of actin filaments: evidence for an actin cortical network at the nuclear inner membrane. PLoS Biol 2, E231.

Holaska JM, Rais-Bahrami S, Wilson KL (2006). Lmo7 is an emerin-binding protein that regulates the transcription of emerin and many other muscle-relevant genes. Hum Mol Genet 15, 3459–3472.

Holaska JM, Wilson KL (2007). An emerin "proteome": purification of distinct emerin-containing complexes from HeLa cells suggests molecular basis for diverse roles including gene regulation, mRNA splicing, signaling, mechanosensing, nuclear architecture. Biochemistry 46, 8897–8908.

Iguchi S, Iwasaki T, Fukami Y, Tokmakov AA (2013). Unlaid *Xenopus* eggs degrade by apoptosis in the genital tract. BMC Cell Biol 14, 11.

Janin A, Bauer D, Ratti F, Millat G, Mejat A (2017). Nuclear envelopathies: a complex LINC between nuclear envelope and pathology. Orphanet J Rare Dis 12, 147.

Jevtic P, Edens LJ, Li X, Nguyen T, Chen P, Levy DL (2015). Concentration-dependent effects of nuclear lamins on nuclear size in *Xenopus* and mammalian cells. J Biol Chem 290, 27557–27571.

Jevtic P, Levy DL (2014). Mechanisms of nuclear size regulation in model systems and cancer. Adv Exp Med Biol 773, 537–569.

Jevtic P, Levy DL (2015). Nuclear size scaling during *Xenopus* early development contributes to midblastula transition timing. Curr Biol 25, 45–52.

Johnson CE, Freel CD, Kornbluth S (2010). Features of programmed cell death in intact *Xenopus* oocytes and early embryos revealed by near-infrared fluorescence and real-time monitoring. Cell Death Differ 17, 170–179.

Kauffmann E, Darnton NC, Austin RH, Batt C, Gerwert K (2001). Lifetimes of intermediates in the beta -sheet to alpha -helix transition of beta-lactoglobulin by using a diffusional IR mixer. Proc Natl Acad Sci USA 98, 6646–6649.

Knight JB, Vishwanath A, Brody JP, Austin RH (1998). Hydrodynamic focusing on a silicon chip: mixing nanoliters in microseconds. Phys Rev Lett 80, 3863–3866.

Koch AJ, Holaska JM (2014). Emerin in health and disease. Semin Cell Dev Biol 29, 95–106.

Komeya M, Hayashi K, Nakamura H, Yamanaka H, Sanjo H, Kojima K, Sato T, Yao M, Kimura H, Fujii T, Ogawa T (2017). Pumpless microfluidic system driven by hydrostatic pressure induces and maintains mouse spermatogenesis in vitro. Sci Rep 7, 15459.

Kranzusch PJ, Lee AS, Berger JM, Doudna JA (2013). Structure of human cGAS reveals a conserved family of second-messenger enzymes in innate immunity. Cell Rep 3, 1362–1368.

Lammerding J, Fong LG, Ji JY, Reue K, Stewart CL, Young SG, Lee RT (2006). Lamins A and C but not lamin B1 regulate nuclear mechanics. J Biol Chem 281, 25768–25780.

Lammerding J, Hsiao J, Schulze PC, Kozlov S, Stewart CL, Lee RT (2005). Abnormal nuclear shape and impaired mechanotransduction in emerin-deficient cells. J Cell Biol 170, 781–791.

Lammerding J, Schulze PC, Takahashi T, Kozlov S, Sullivan T, Kamm RD, Stewart CL, Lee RT (2004). Lamin A/C deficiency causes defective nuclear mechanics and mechanotransduction. J Clin Invest 113, 370–378.

Le HQ, Ghatak S, Yeung CY, Tellkamp F, Gunschmann C, Dieterich C, Yeroslaviz A, Habermann B, Pombo A, Niessen CM, Wickstrom SA (2016). Mechanical regulation of transcription controls Polycomb-mediated gene silencing during lineage commitment. Nat Cell Biol 18, 864–875.

Lee KK, Haraguchi T, Lee RS, Koujin T, Hiraoka Y, Wilson KL (2001). Distinct functional domains in emerin bind lamin A and DNA-bridging protein BAF. J Cell Sci 114, 4567–4573.

Levy DL, Heald R (2010). Nuclear size is regulated by importin alpha and Ntf2 in *Xenopus*. Cell 143, 288–298.

Markiewicz E, Tilgner K, Barker N, van de Wetering M, Clevers H, Dorobek M, Hausmanowa-Petrusewicz I, Ramaekers FC, Broers JL, Blankesteijn WM, *et al.* (2006). The inner nuclear membrane protein emerin regulates beta-catenin activity by restricting its accumulation in the nucleus. EMBO J 25, 3275–3285.

Neelam S, Chancellor TJ, Li Y, Nickerson JA, Roux KJ, Dickinson RB, Lele TP (2015). Direct force probe reveals the mechanics of nuclear homeostasis in the mammalian cell. Proc Natl Acad Sci USA 112, 5720–5725.

Newport J, Kirschner M (1982). A major developmental transition in early *Xenopus* embryos: II. Control of the onset of transcription. Cell 30, 687–696.

Pajerowski JD, Dahl KN, Zhong FL, Sammak PJ, Discher DE (2007). Physical plasticity of the nucleus in stem cell differentiation. Proc Natl Acad Sci USA 104, 15619–15624.

Peshkin L, Wuhr M, Pearl E, Haas W, Freeman RM, Jr, Gerhart JC, Klein AM, Horb M, Gygi SP, Kirschner MW (2015). On the relationship of protein and mRNA dynamics in vertebrate embryonic development. Dev Cell 35, 383–394.

Pfaff J, Rivera Monroy J, Jamieson C, Rajanala K, Vilardi F, Schwappach B, Kehlenbach RH (2016). Emery-Dreifuss muscular dystrophy mutations impair TRC40-mediated targeting of emerin to the inner nuclear membrane. J Cell Sci 129, 502–516.

Prokocimer M, Davidovich M, Nissim-Rafinia M, Wiesel-Motiuk N, Bar DZ, Barkan R, Meshorer E, Gruenbaum Y (2009). Nuclear lamins: key regulators of nuclear structure and activities. J Cell Mol Med 13, 1059–1085.

Raab M, Gentili M, de Belly H, Thiam HR, Vargas P, Jimenez AJ, Lautenschlaeger F, Voituriez R, Lennon-Dumenil AM, Manel N, Piel M (2016). ESCRT III repairs nuclear envelope ruptures during cell migration to limit DNA damage and cell death. Science 352, 359–362.

Razafsky D, Hodzic D (2009). Bringing KASH under the SUN: the many faces of nucleo-cytoskeletal connections. J Cell Biol 186, 461–472.

Reil M, Dabauvalle MC (2013). Essential roles of LEM-domain protein MAN1 during organogenesis in *Xenopus laevis* and overlapping functions of emerin. Eur J Cell Biol 92, 280–294.

Rowat AC, Lammerding J, Ipsen JH (2006). Mechanical properties of the cell nucleus and the effect of emerin deficiency. Biophys J 91, 4649–4664.

Salpingidou G, Smertenko A, Hausmanowa-Petrucewicz I, Hussey PJ, Hutchison CJ (2007). A novel role for the nuclear membrane protein emerin in association of the centrosome to the outer nuclear membrane. J Cell Biol 178, 897–904.

Samson C, Celli F, Hendriks K, Zinke M, Essawy N, Herrada I, Arteni AA, Theillet FX, Alpha-Bazin B, Armengaud J, *et al.* (2017). Emerin self-assembly mechanism: role of the LEM domain. FEBS J 284, 338–352.

Segura-Totten M, Kowalski AK, Craigie R, Wilson KL (2002). Barrier-to-auto-integration factor: major roles in chromatin decondensation and nuclear assembly. J Cell Biol 158, 475–485.

Shimi T, Koujin T, Segura-Totten M, Wilson KL, Haraguchi T, Hiraoka Y (2004). Dynamic interaction between BAF and emerin revealed by FRAP, FLIP, and FRET analyses in living HeLa cells. J Struct Biol 147, 31–41.

Shimojima M, Yuasa S, Motoda C, Yozu G, Nagai T, Ito S, Lachmann M, Kashimura S, Takei M, Kusumoto D, *et al.* (2017). Emerin plays a crucial role in nuclear invagination and in the nuclear calcium transient. Sci Rep 7, 44312.

Stephens AD, Banigan EJ, Adam SA, Goldman RD, Marko JF (2017). Chromatin and lamin A determine two different mechanical response regimes of the cell nucleus. Mol Biol Cell 28, 1984–1996.

Stiles T, Fallon R, Vestad T, Oakey J, Marr DWM, Squier J, Jimenez R (2005). Hydrodynamic focusing for vacuum-pumped microfluidics. Microfluid Nanofluid 1, 280–283.

Sullivan T, Escalante-Alcalde D, Bhatt H, Anver M, Bhat N, Nagashima K, Stewart CL, Burke B (1999). Loss of A-type lamin expression compromises nuclear envelope integrity leading to muscular dystrophy. J Cell Biol 147, 913–920.

Tapley EC, Starr DA (2013). Connecting the nucleus to the cytoskeleton by SUN-KASH bridges across the nuclear envelope. Curr Opin Cell Biol 25, 57–62.

Tokmakov AA, Iguchi S, Iwasaki T, Fukami Y (2011). Unfertilized frog eggs die by apoptosis following meiotic exit. BMC Cell Biol 12, 56.

Vargas JD, Hatch EM, Anderson DJ, Hetzer MW (2012). Transient nuclear envelope rupturing during interphase in human cancer cells. Nucleus 3, 88–100.

Vukovic LD, Jevtic P, Zhang Z, Stohr BA, Levy DL (2016). Nuclear size is sensitive to NTF2 protein levels in a manner dependent on Ran binding. J Cell Sci 129, 1115–1127.

Willer MK, Carroll CW (2017). Substrate stiffness-dependent regulation of the SRF-Mkl1 co-activator complex requires the inner nuclear membrane protein Emerin. J Cell Sci 130, 2111–2118.

Willis J, DeStephanis D, Patel Y, Gowda V, Yan S (2012). Study of the DNA damage checkpoint using *Xenopus* egg extracts. J Vis Exp 2012, e4449.

Wilson KL, Foisner R (2010). Lamin-binding Proteins. Cold Spring Harb Perspect Biol 2, a000554.

Wolin SL, Krohne G, Kirschner MW (1987). A new lamin in *Xenopus* somatic tissues displays strong homology to human lamin A. EMBO J 6, 3809–3818.

Worman HJ, Ostlund C, Wang Y (2010). Diseases of the nuclear envelope. Cold Spring Harb Perspect Biol 2, a000760.

Xia Y, Whitesides GM (1998). Soft lithography. Annu Rev Mater Sci 28, 153–184.

Yamamoto Y, Sakisaka T (2012). Molecular machinery for insertion of tail-anchored membrane proteins into the endoplasmic reticulum membrane in mammalian cells. Mol Cell 48, 387–397.

Zhou X, Lau L, Lam WW, Au SW, Zheng B (2007). Nanoliter dispensing method by degassed poly(dimethylsiloxane) microchannels and its application in protein crystallization. Anal Chem 79, 4924–4930.

Zuela N, Gruenbaum Y (2016). Matefin/SUN-1 phosphorylation on serine 43 is mediated by CDK-1 and required for its localization to centrosomes and normal mitosis in *C. elegans* embryos. Cells 5, E8.